Journal of Power Sources 195 (2010) 3621–3630

Contents lists available at ScienceDirect

Journal of Power Sources

journal homepage: www.elsevier.com/locate/jpowsour

Analysis of operating parameters considering flow orientation for the performance of a proton exchange membrane fuel cell using the Taguchi method

Horng-Wen Wu*, Hui-Wen Gu

Department of System and Naval Mechatronic Engineering, National Cheng Kung University, 1 Ta-Hsueh Road, Tainan 701, Taiwan, ROC

ARTICLE INFO

Article history:
Received 24 September 2009
Received in revised form
20 November 2009
Accepted 25 November 2009
Available online 4 December 2009

Keywords:
Proton exchange membrane fuel cell
Taguchi method
Operating parameters
Flow orientation

ABSTRACT

This study has applied the L_{18} 2×3^7 orthogonal array of the Taguchi method to determine the optimal combination of six primary operating parameters (flow orientation, temperature of fuel cell, anode and cathode humidification temperatures, anode, and cathode stoichiometric flow ratios) of a PEM fuel cell. The optimal combination factor is co-flow, a cell temperature of 333 K, an anode humidification temperature of 353 K, a cathode humidification temperature of 333 K, a stoichiometric flow ratio for hydrogen of 2, and a stoichiometric flow ratio for oxygen of 3; and the amount of maximum power is 17.61 W. The results for the experiment indicate that flow orientation, temperature of fuel cell, and anode and cathode humidification temperatures are significant factors for affecting the performance. Furthermore, this study simulates the transport phenomenon and electrochemical reactions using a finite-element method at the optimal combination factor from the experimental results of Taguchi method.

1. Introduction

The major advantages of proton exchange membrane fuel cell (PEMFC) are low-temperature operation, high efficiency, no emission, low noise, and quick starting to high energy and current density under room temperature. The performance of the fuel cell depends on the kinetics of the electrochemical process and performance of the components. Excessive local cell temperature due to insufficient or non-effective cell cooling may cause membrane dehydration, shrinking or even rupture. Hence, the thermal and water management issues are strongly coupled and they have a direct impact on cell performance [1].

The most recent models addressed two or more of the thermal and water management [2–8]. Nguyen and White [2] developed two-dimensional heat and water transport models that accounted for variation in temperature and membrane hydration conditions along the flow channels. Singh et al. [3] presented two-dimensional analysis of mass transport in PEM fuel cells. Hwang [4] found that the fluid-phase and solid-matrix temperature distributions were significantly affected by the flow orientation in the PEM fuel cell. Replacing the parallel-flow geometry by the counter-flow geometry had an advantage of reducing the local maximum temperature inside the fuel cell. Jang et al. [5] developed a two-dimensional numerical model to investigate the performance of the PEM fuel cells. Parameters used in the analysis included the porosity and thickness of the gas diffuser layer (GDL). Their results showed that increasing the porosity of gas diffusion layer caused the increasing of mass transfer of fuel and air and generated a higher reaction rate. The cell performance with co-flow condition was notably better at lower operating voltage conditions. Guvelioglu and Stenger [6] found that hydrogen and air flow rates and their relative humidity are critical to current density, membrane dry-out, and electrode flooding. Perng and Wu [7] presented that the transverse installation of a baffle plate and a rectangular block in the fuel flow channel can effectively enhance the local cell performance of a PEM fuel cell. Um and Wang [8] used computation fuel cell dynamics framework to develop a unified water transport equation for a PEM fuel cell.

The optimization of the operating parameters affecting the performance of PEM fuel cell and obtaining related data is very important in various applications, and especially for fuel cell producers to validate and improve their models. Therefore doing large number of experiments is often needed to understand clearly how the parameters influence the performance of PEM fuel cell and to optimize them. In terms of the experimental process, most studies used one-factor-at-a-time experiments or full-factorial experiments. However, these approaches suffered from the following chief shortcomings: they frequently generated factor effect bias; multiple experiments are required when analyzing a large number of factors, to the point of failing to perform the experiments effi-

* Corresponding author. Tel.: +886 6 2740718x223; fax: +886 6 2747019.
E-mail address: z7708033@email.ncku.edu.tw (H.-W. Wu).

0378-7753/$ – see front matter © 2009 Elsevier B.V. All rights reserved.
doi:10.1016/j.jpowsour.2009.11.128

Nomenclature

ANOVA	analysis of variance
C	mole concentration ($mol\,m^{-3}$)
$D_{i,eff}$	diffusivity of species i ($m^2\,s^{-1}$)
F	Fraday's constant ($96{,}478\,C\,mol^{-1}$)
i	current density ($A\,m^{-3}$)
K	permeability (m^2)
M	molecular weight ($kg\,mol^{-1}$)
P	pressure of system (Pa)
R_u	gas constant ($8.314\,J\,mol^{-1}\,K^{-1}$)
S	source term
Sa	fuel cell active surface area
S/N	signal-to-noise ratio (dB)
T	temperature (K)
u	inlet velocity of gas in X direction ($m\,s^{-1}$)
V	voltage (V)
v	inlet velocity of gas in Y direction ($m\,s^{-1}$)
α	electric conductivity ($\Omega^{-1}\,m^{-1}$)
β	heat transfer coefficient ($W\,K^{-1}\,m^{-3}$)
ε	porosity
ρ	density of gas ($kg\,m^{-3}$)
μ	viscosity ($m\,s^{-2}$)
ω	mass fraction
κ^{eff}	thermal conductivity ($W\,K^{-1}\,m^{-1}$)
ζ	stoichiometric flow ratio
η	overpotential

Superscript

s	current conductor
τ	coefficient of Bruggeman

Subscript

a	anode
c	cathode
i, j	species

ciently. On the other hand, the design of experiments has received increasing attention.

In recent years, several researchers employed Taguchi method to evaluate the respective impacts of those parameters on the performance of PEM fuel cell and to reduce the number of experiments when they studied many parameters [9–15]. Grujicic and Chittajallu [9,10] applied a two-dimensional model coupled with a nonlinear constrained optimization algorithm to determine an optimum design of the fuel cell for the operation and the geometrical parameters of cathode such as the air inlet pressure, the cathode thickness, and length and the width of shoulders in the interdigitated air distributor. Yu et al. [11] used the method of the design of experiments (DOE) to obtain the optimal combination of the six primary operating parameters (fuel cell operating temperatures, operating pressures, anode and cathode humidification temperatures, anode and cathode stoichiometric flow ratios). In the first stage, they adopted a 2^{k-2} fractional factorial design of the DOE to determine whether these factors significantly influence a response and the interactions between various parameters. Second, the L_{27} (3^{13}) orthogonal array of the Taguchi method was employed to determine the optimal combination of factors for a fuel cell. Wu et al. [12] applied the Taguchi method to acquire the primary optimums of the operating parameters in the PEM fuel cell. Each row in the orthogonal array together with its relative responses was used to establish a set of training patterns (input/target pair) to the neural network. Kaytakoğlu and Akyalın [13] employed the Taguchi's orthogonal array (OA) L_9 (3^4) to determine optimum working conditions (system pressure, flow rate ratio of H_2 and O_2, temperature of fuel cell and temperature of humidifiers) in obtaining maximum power density of a PEM fuel cell. Torchio et al. [14] applied it to operation parameter effect investigation on the cogenerative performance of a PEM fuel cell stack, through a statistical methodology used for the experimental data analysis by 2^4 factorial design (four parameters, each at two levels, were anode and cathode flow inlet temperature; cathode flow dew point temperature; cathode flow stoichiometry to run all $2^4 = 16$ treatment combinations). Dante et al. [15] used a fractional experimental design supported by a statistical methodology to analyze how four parameters (hydrogen and oxygen pressures and flow rates, each at two levels, eight treatment combinations) affected the electric power output of a stack.

Many researchers have studied how operating parameters affect the performance of the fuel cells by experiments and analyses. However, there are few studies applied the Taguchi method to optimization analysis of operating parameters considering flow orientation with operating temperatures, humidification temperatures, and flow rate of reactant gases. Hence, the objective of this paper is to apply the Taguchi's orthogonal array L_{18} (2×3^7) with experiment to determine the optimal operating condition of these operating parameters and then to realize the transport phenomenon by two-dimensional simulation models for the fuel cell performance at the optimal operating condition. The results of this paper may be of interest to engineers attempting to develop the optimization of a PEM fuel cell performance and to researchers interested in the transport phenomenon corresponding to the optimization condition in the PEM fuel cell.

2. Experimental system

A schematic drawing of the experimental apparatus employed in this study is shown in Fig. 1. The apparatus includes fuel supply system, flow rate control system, temperature control system, humidifying system, and electronic load system. The active surface area of the signal PEM fuel cell used in this study is $5 \times 5\,cm^2$. The membrane-electrode-assembly (MEA) of the fuel cell has a five-layer structure combining a proton exchange membrane with a catalyst layer and gas diffusion layer. The single serpentine channel width and the rib width of the flow fields were 1.5 mm and tested on both the anode and cathode side. The experiment was performed for two patterns: the co-flow and the counter-flow.

This study employs the Taguchi method in the experiment with different PEM fuel cell operating conditions. The Taguchi method offers two new powerful elements. First, it is a disciplined way of improving product and process quality with unprecedented success. Second, it provides a means to cost less for investigating the available alternatives. Although Taguchi method was built upon well developed concepts of optimization through the design of experiments, his philosophy emphasizes designing the quality improvement practices into the procedure for carrying out experiments.

The steps of the Taguchi method include the following [16].

2.1. Describe quality characteristics and design parameters

Quality characteristics selected to be the optimization criteria are divided into three categories, the larger-the-best, the smaller-the-best and the nominal-the-best. The quality characteristic of this study is the maximum electrical power of PEM fuel cell, which belongs to a larger-the-best characteristic, and is calculated by using:

$$\frac{S}{N} = -10 \log \frac{1}{n} \left(\sum_{i=1}^{n} \frac{1}{y_i^2} \right) \quad (1)$$

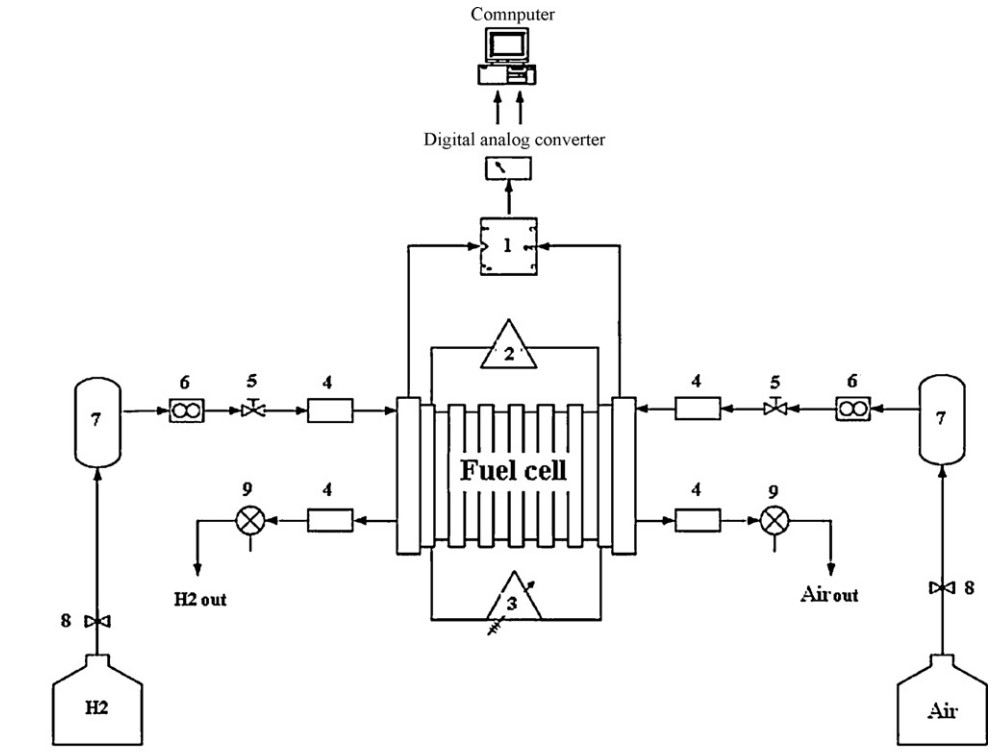

Fig. 1. Fuel cell test system.

where y_i is the value of quality characteristic measured from the trial and the unit of S/N is dB; n is the number of the tests in a trial.

2.2. Design and conduct the experiments

The experimental design factors considered are: (A) flow orientation, (B) temperature of fuel cell, (C) anode humidification temperature, (D) cathode humidification temperature, (E) stoichiometric flow ratio of hydrogen, and (F) stoichiometric flow ratio of oxygen.

Taguchi's arrays are versatile recipes that are applied to several experimental conditions. The experiments were designed according to the orthogonal array technique. An orthogonal array is a fractional factorial design with pair wise balancing property. Using orthogonal array design can estimate how multiple process variables affect the performance characteristic simultaneously while minimizing the number of test runs. The three-level orthogonal arrays most often used in practice are L_9 (3^4), L_{18} (2×3^7), L_{27} (3^{13}), L_{36} ($2^{11} \times 3^{12}$), L_{36} ($2^3 \times 3^{13}$) and L_{54} ($2^1 \times 3^{25}$). In this paper, we used the L_{18} (2×3^7), the minimum orthogonal array for six parameters. To observe the data reliably on this experiment, this study repeated each one two times with same conditions.

2.3. Analyze the results to determine the optimum conditions

The results of the Taguchi experiments are analyzed in a standard series of phases. First, the main effects are evaluated and the influences of the factors are determined in qualitative terms. The optimum condition and performance at the optimum condition are also determined from the factorial effects. In the next phase, analysis of variance (ANOVA) is performed on the experimental data. ANOVA study identifies the relative influence of the factors in discrete terms.

According to the six main control factors and each at three levels, obtaining signal-to-noise ratios (S/N) of the experiment results after selecting the proper orthogonal arrays identifies the relationship between the parameters and the responses (the maximum electrical power on the fuel cell), and obtains the primary optimums of the operating parameters. This study uses the ANOVA to identify the important parameters that can affect fuel cell quality characteristics and determines the most robust set of operating conditions from variations within the results. In Table 3, the F-test of statistics is used to decide which parameters of the fuel cell influence the quality characteristics significantly.

2.4. Run a confirmatory test using the optimum conditions

In order to test the predicted result, we have conducted confirmation experiment by running another two replications at the optimal settings of the process parameters determined from the analysis. From the analyses of S/N ratio and the mean response characteristic, the optimum levels of the control factors are determined as: $A1$, $B2$, and $D2$. Hence, the predicted mean of the quality characteristic (power) has been computed as shown in the reference [17]:

$$\hat{SN} = \bar{T} + (\overline{A1} - \bar{T}) + (\overline{B2} - \bar{T}) + (\overline{C3} - \bar{T}) + (\overline{D2} - \bar{T}) \quad (2)$$

where $\bar{T}$ is the total S/N average for all experiment data. $A1$, $B2$, $C3$, and $D2$ are the average values of the S/N with process parameters at

their respective optimal levels. Substituting these in Eq. (2) yields the mean optimum value of the S/N as $\widehat{SN} = 24.7$ dB.

An important step in Taguchi's optimization technique is to conduct confirmation experiments for validating the predicted results. Thus a 95% confidence interval (CI) for the predicted mean of optimum quality characteristic on a confirmation test is estimated using the following two equations:

$$CI = \sqrt{F(\alpha, 1, f_e)V_e\left[\frac{1}{N_{eff}} + \frac{1}{R}\right]} \quad (3)$$

and

$$N_{eff} = \frac{N}{1 + T_{DOF}} \quad (4)$$

where $F(\alpha, 1, f_e)$ is the F-ratio required for $100(1-\alpha)$ percent confidence interval, f_e is DOF for error, V_e = Error variance, R is number of replications for confirmation experiment, and N_{eff} is effective number of replications. N is the total number of experiments and T_{DOF} is the total degrees of freedom for the estimate of mean optimum.

After substituting these values in Eqs. (3) and (4), the confidence interval is CI = ±1.31. The 95% confidence limits of the predicted optimal power is thus obtained as 25.49 ± 1.31 dB. In order to test the predicted result, we have conducted confirmation experiment by running another two replications at the optimal settings of the process parameters determined from the analysis. The S/N of the mean power from the confirmation experiments is 24.9 dB, which falls within the predicted 95% confidence interval. Therefore, the predictions made by Taguchi's parameter design technique were in good agreement with the confirmation results.

3. Numerical model

Two-dimensional module of fuel cell module is in y–z plane as shown in Fig. 2. The domain of this module comprises two gas diffusion layers, two catalyst layers and a proton exchange membrane.

3.1. Assumptions

The present model is established under the following assumptions:

1. Flow is laminar everywhere due to small gas pressure gradient and low Reynolds number.
2. Reactant gases behave according to the ideal gas model.
3. The electrodes and membrane are made of homogeneous materials.
4. Water in the fuel cell exists only in the gas phase.
5. Polymer electrolyte membrane is impermeable to reactant gas.
6. Proton can only transport through the electrolyte, and the electron through the solid carbon phase.
7. Three species including oxygen, water and nitrogen are considered on the cathode side while only hydrogen and water are considered on the anode side.

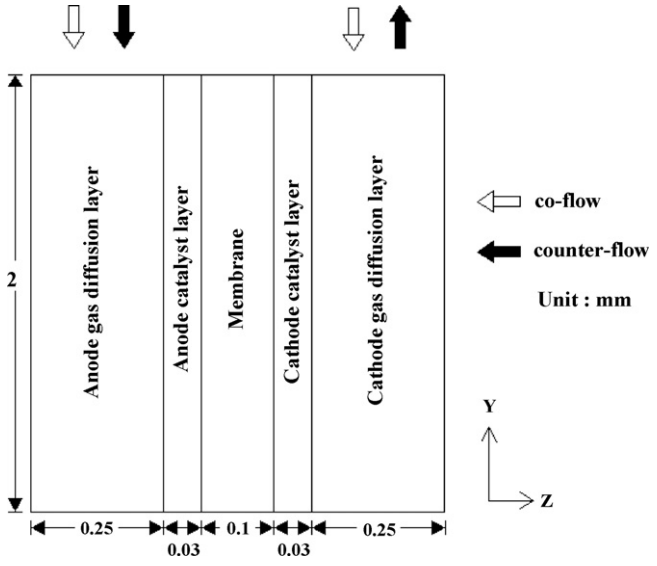

Fig. 2. Two-dimensional model of fuel cell module.

3.2. Governing equations

3.2.1. Momentum and mass transports

The Brinkman-extended Darcy's equation together with the mass conservation equation describes the fluid flow in the porous media.

Brinkman-extended Darcy's law:

$$\rho\vec{u}\cdot\nabla\vec{u} = -\nabla P + \nabla\cdot\left(\mu\nabla\vec{u}\right) + S_m \quad (5)$$

Continuity equation:

$$\nabla\left(\rho\vec{u}\right) = 0 \quad (6)$$

where ρ is the density, μ is the viscosity, $\vec{u}$ is the velocity vector, and P is the pressure. The source term in the momentum equations is added according to Darcy's law, representing an extra drag force proportional to fluid viscosity and velocity, and inversely proportional to the permeability of a porous medium, i.e., $S_m = -(\mu/\kappa)u$, where κ is the permeability.

3.2.2. Species transports

Momentum balance is coupled with mass balance through Maxwell–Stefan equation which is a better approximation than Fick's Law for inter-diffusion of species and multi component transport, given by:

Stefan–Maxwell equation:

$$\rho_{mix}\vec{u}\cdot\nabla\omega_i = \nabla\cdot\left\{\rho_{mix}\omega_i\sum_{j=1}^{N}D_{i,eff,j}\left[\frac{M}{M_j}\left(\nabla\omega_j + \omega_j\frac{\nabla M}{M}\right) + \left(\chi_j - \omega_j\right)\frac{\nabla P}{P}\right]\right\} + S_i \quad (7)$$

The model takes into account two species in the anode as H_2 and H_2O and three species in the cathode as O_2, H_2O, and N_2. Eq. (4) is solved for mass fraction of H_2 at the anode and mass fractions of O_2 and H_2O at the cathode while mass fractions of H_2O at anode and N_2 at the cathode are calculated such that total mass fractions at each domain is unity. The source terms S_i are implemented on the basis of electrochemical kinetics, i.e., consuming the reactant to produce the current.

According to the Bruggman model [18], the effective diffusivity of the species i in the porous electrode is expressed as:

$$D_{i,eff} = \varepsilon^{\tau}D_i \quad (8)$$

On the gas diffusion layer:

$$S_i = 0 \quad (9)$$

On the catalyst layer of the anode:

$$S_{H_2} = -i_a\frac{M_{H_2}}{2F} \quad (10)$$

Table 1
Control factors and levels for the L_{18} (2×3^7) design.

Factor	Parameters	Level 1	Level 2	Level 3
A	Flow orientation	Co-flow	Counter-flow	
B	Temperature of fuel cell (K)	313	333	353
C	Anode humidification temperature (K)	313	333	353
D	Cathode humidification temperature (K)	313	333	353
E	Stoichiometric flow ratio of hydrogen	1	2	3
F	Stoichiometric flow ratio of oxygen	1	2	3

On the catalyst layer of the cathode side:

$$S_{O_2} = -i_c \frac{M_{O_2}}{4F}, \quad S_{H_2O} = -i_c \frac{M_{H_2O}}{2F} \tag{11}$$

3.2.3. Thermal transport

Conservation of energy for any domain in a PEM fuel cell is described by:

$$(\rho C_p)_f (u \cdot \nabla T) = \nabla \cdot (k_{eff} \nabla T) + S_T \tag{12}$$

where C_p is the mixture-averaged specific heat capacity and k_{eff} is the effective thermal conductivity. The source term in the energy conservation equation includes the heat released by the electrochemical reaction:

$$S_T = \left[\frac{T(-\Delta s)}{n_e F} + \eta \right] \cdot i \tag{13}$$

Heat transfer in the membrane is governed by:

$$\nabla \cdot (k_{mem} \cdot \nabla T) = 0 \tag{14}$$

3.2.4. Current transport

The continuity of current in a conducting material is described by:

$$\nabla \cdot i = 0 \tag{15}$$

In the catalyst layer of a PEM fuel cell, the porous matrix contains two kinds of solid phases, i.e., ionic conductor (electrolyte) and electronic conductor (catalyst). Protons travel through the ionic conductor (the membrane) to form an ionic current denoted by i_e, while electrons can only be transferred through the solid matrix of electrodes which results in an electronic current denoted by i_s. The continuity equation of current then becomes:

$$\nabla \cdot i = \nabla \cdot i_e + \nabla \cdot i_s \tag{16}$$

i_e and i_s are the currents flowing through the catalyst and the electrolyte, respectively. Because the electrodes are electroneutral everywhere, there is no charge buildup in the catalyst layers. The potential equations for both solid and electrolyte phases are obtained by applying Ohmic's law to Eq. (16):

$$\nabla \cdot (-\sigma_{s,eff} \nabla \phi_s) = S_s \tag{17}$$

$$\nabla \cdot (-\sigma_{e,eff} \nabla \phi_e) = S_e \tag{18}$$

Table 2
Experimental results obtained at cell potential of 0.5 V for the L_{18} (2×3^7) design.

Orthogonal array: L_{18} ($2^1 \times 3^7$)									Power (W)		Average power (W)	S/N (dB)
Exp.	*A*	*B*	*C*	*D*	*E*	*F*	*e*	*e*	Y1	Y2		
1	1	1	1	1	1	1	1	1	11.78	11.30	11.54	21.24
2	1	1	2	2	2	2	2	2	16.08	16.14	16.11	24.14
3	1	1	3	3	3	3	3	3	17.66	17.74	17.70	24.96
4	1	2	1	1	2	2	3	3	14.42	14.46	14.44	23.19
5	1	2	2	2	3	3	1	1	17.46	17.44	17.45	24.84
6	1	2	3	3	1	1	2	2	17.18	17.05	17.12	24.67
7	1	3	1	2	1	3	2	3	13.66	13.69	13.68	22.72
8	1	3	2	3	2	1	3	1	13.90	13.93	13.92	22.87
9	1	3	3	1	3	2	1	2	12.44	12.42	12.43	21.89
10	2	1	1	3	3	2	2	1	16.24	16.27	16.26	24.22
11	2	1	2	1	1	3	3	2	11.77	11.73	11.75	21.40
12	2	1	3	2	2	1	1	3	16.10	16.22	16.16	24.17
13	2	2	1	2	3	1	3	2	14.01	14.60	14.31	23.10
14	2	2	2	3	1	2	1	3	11.58	11.46	11.52	21.23
15	2	2	3	1	2	3	2	1	15.49	15.55	15.52	23.82
16	2	3	1	3	2	3	1	2	12.03	11.89	11.96	21.55
17	2	3	2	1	3	1	2	3	8.49	9.83	9.16	19.17
18	2	3	3	2	1	2	3	1	13.26	13.28	13.27	22.46

Table 3
ANOVA for the L_{18} (2×3^7) design in Table 2.

Factor	SS	DOF	Var.	*F*	$F_{0.06}$	*P*	SS′	Contribution
A	4.90	1	4.90	6.76	4.79	0.03	4.18	10.00%
B	10.78	2	5.39	7.43	4.08	0.01	9.33	22.34%
C	6.11	2	3.06	4.21	4.08	0.06	4.66	11.17%
D	10.89	2	5.44	7.50	4.08	0.01	9.44	22.60%
E	3.27	2	1.63	2.25	4.08	0.17	–	–
F	(1.38)	(2)	–	–	–	–	–	–
e	(2.75)	(4)	–	–	–	–	–	–
Error	5.80	8	0.73	Confidence level: 94%			14.15	33.88%
Total	41.75	17					41.75	100.00%

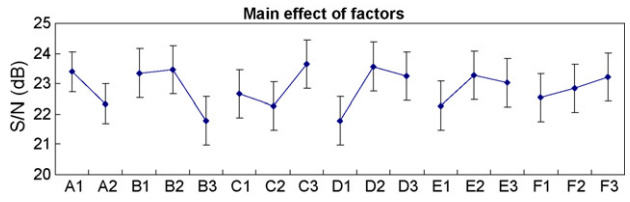

Fig. 3. S/N response for the L_{18} (2×37) design.

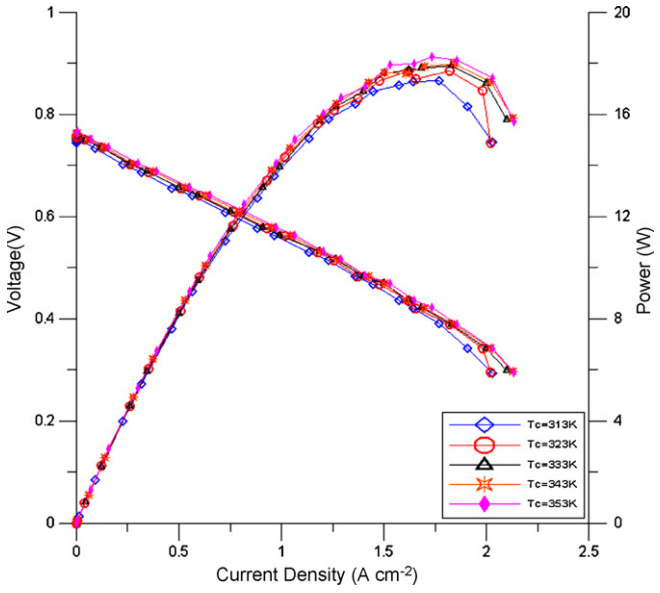

Fig. 4. Variation of voltage and power with cathode humidification temperature for various current densities and other parameters at the optimum condition (*A1B2C3E2F3*).

The source terms in the electron and proton transport equations, i.e., Eqs. (17) and (18), result from the electrochemical reaction occurring in the catalyst layers of anode and cathode sides.

Anode catalyst layer:

$$S_e = i_a; \quad S_s = -i_a \tag{19}$$

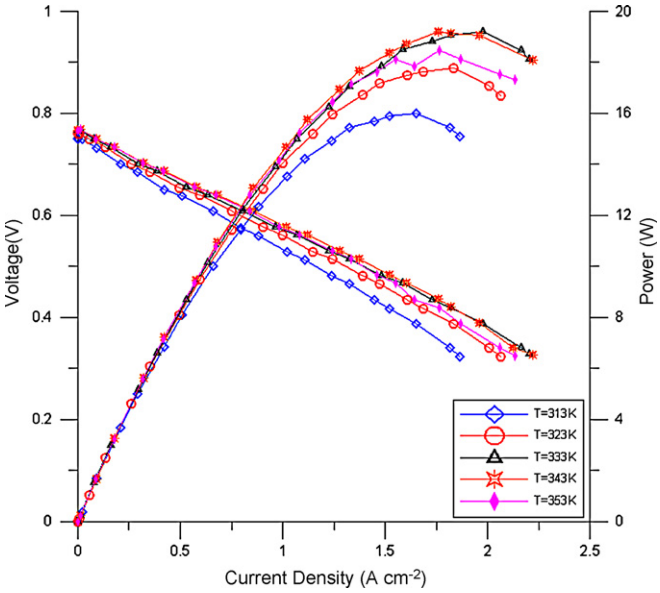

Fig. 5. Influence of cell temperature on voltage and power with various current densities and other parameters at the optimum condition (*A1C3D2E2F3*).

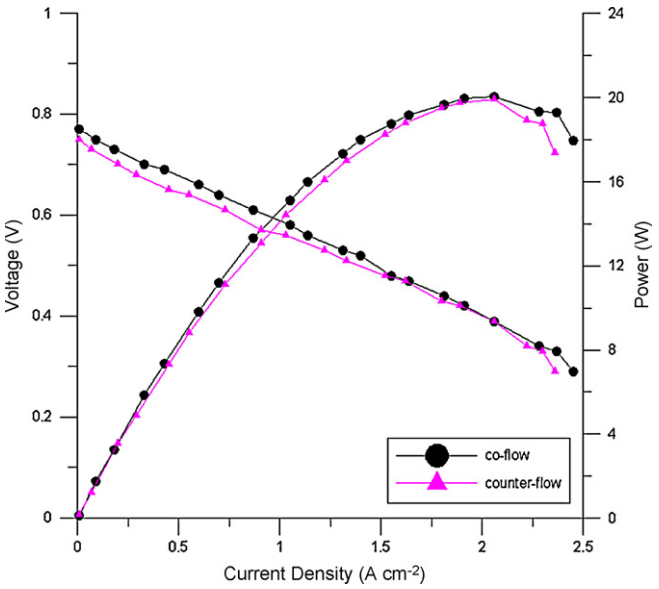

Fig. 6. Variation of voltage and power with flow orientation for various current densities and other parameters at the optimum condition (*B2C3D2E2F3*).

Cathode catalyst layer:

$$S_e = i_c; \quad S_s = -i_c \tag{20}$$

$$i_a = i_{a,0}\left\{\left(\frac{C_{H_2}}{C_{H_{2,eff}}}\right)^2 \exp\left[\frac{4\alpha_a F}{R_u T}\eta\right]\right\} \tag{21}$$

$$i_c = i_{c,0}\left\{\left(\frac{C_{O_2}}{C_{O_{2,eff}}}\right)^2 \exp\left[\frac{4\alpha_a F}{RT}\eta\right] - \left(\frac{C_{H_2O}}{C_{H_2O_{eff}}}\right)^2 \exp\left[\frac{4(1-\alpha_c)F}{R_u T}\eta\right]\right\} \tag{22}$$

where i_a and i_c are obtained from the Butler–Volmer equation which describes the relationship among the local transfer current density, the reactant concentrations, and phase potentials.

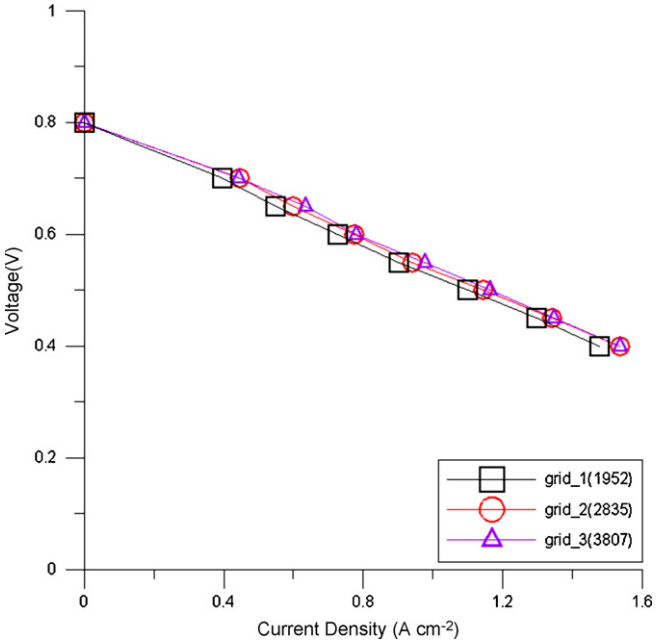

Fig. 7. Comparison of predictions for various grid systems.

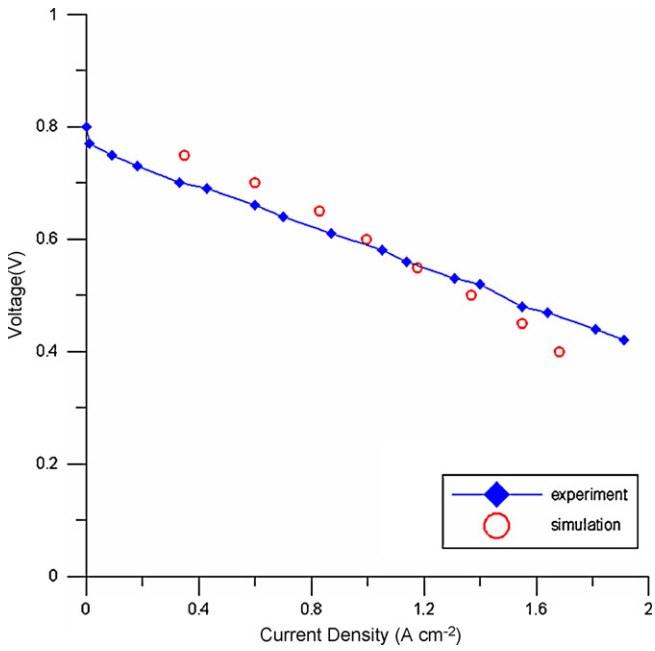

Fig. 8. Comparison of the results between the present prediction and experiment at the optimal condition (*A1B2C3D2E2F3*).

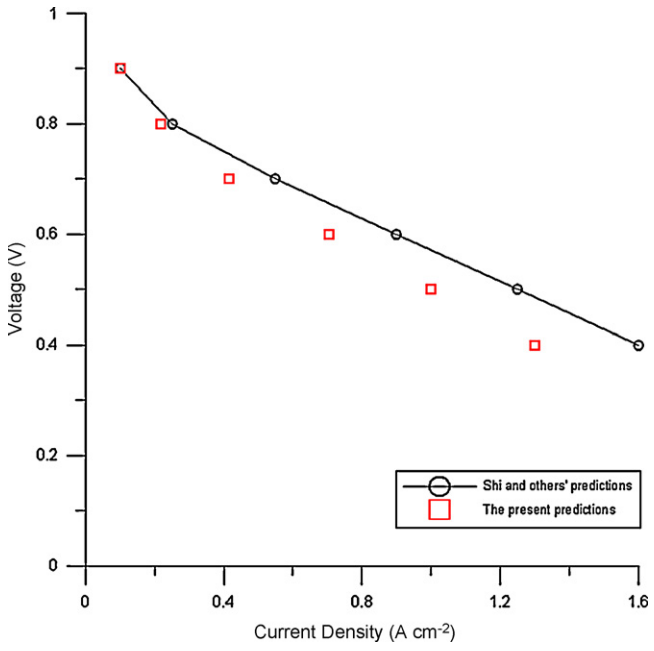

Fig. 9. Comparison of the results between the present prediction and Shi, Wang, and Zhang's prediction.

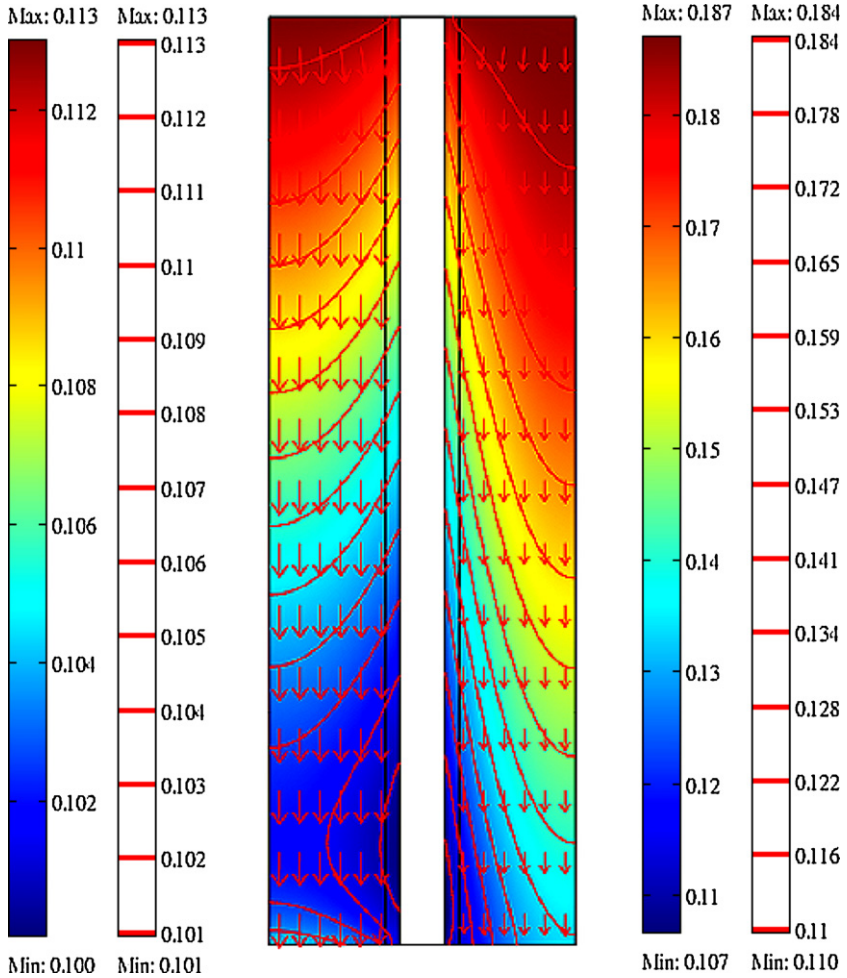

Fig. 10. Oxygen and Hydrogen concentration profiles for V_{cell} = 0.5 V at the optimal condition (*A1B2C3D2E2F3*).

3.3. Boundary conditions

The boundary conditions are required only at the external surfaces of the computational domain due to the single-domain formulation used. At the fuel and oxidant inlets, the following conditions are prescribed by:

$$u_{a,in} = \zeta_a \frac{I_{ref} Sa}{4F} \frac{R_u T}{P_a} \frac{1}{X_{H_2}}, \quad u_{c,in} = \zeta_c \frac{I_{ref} Sa}{4F} \frac{R_u T}{P_c} \frac{1}{X_{O_2}} \tag{23}$$

The inlet velocities of fuel and oxidant can be also expressed by their respective stoichiometric flow ratios, i.e., ζ at 1 A cm^{-2}. Both outlets of the module have an ambient pressure. The anode is supplied with the humidified hydrogen of mass fractions of 11.3%/88.7% for H_2/H_2O at 353 K. The cathode side feeds with the saturated air of 18.7%/6.4%/74.9% for $O_2/H_2O/N_2$, where N_2 is considered as an inert gas and serves as diluents. The boundary conditions for the phase potential at the interface between the catalyst layer and the membrane are $\Phi = 0$ at the anode side, and $\partial\Phi/\partial X = 0$ at the cathode side. Because the phase potential is a linear distribution in the membrane, the phase potential boundary condition can be written as $\partial\Phi/\partial Y = 0$.

4. Results and discussion

4.1. Experimental analysis

The experimental design factors considered are: (*A*) flow orientation, (*B*) temperature of fuel cell, (*C*) anode humidification temperature, (*D*) cathode humidification temperature, (*E*) stoichiometric flow ratio of hydrogen, and (*F*) stoichiometric flow ratio of oxygen (Table 1); the response is the output power which is tested twice to calculate the average value (Table 2). The orthogonal experimental design can separate out how each control factor affects the S/N at different levels.

Fig. 3 shows the S/N response graph derived from the factors at different levels from Table 2. The larger-the-best performance characteristic, Eq. (1), has been taken in obtaining the maximum electrical power of PEMFC. The order of graphs in Fig. 3 prepared for the experiments is according to how the parameters influence the performance characteristics. The optimal level of a process parameter in obtaining the maximum electrical power is the level with the highest S/N value calculated by Eq. (1). The size of the S/N is positively related to the quality characteristic. The greatest S/N from these levels obtained is the primary optimal combination of the control factor levels, *A*1 (the co-flow), *B*2 (temperature of 333 K), *C*3 (the anode humidification temperature of 353 K), *D*2 (the cathode humidification temperature of 333 K), *E*2 (the hydrogen stoichiometric flow ratio of 2), and *F*3 (the oxygen stoichiometric flow ratio of 3).

The optimal combination of process parameters can be predicted with the ANOVA on the performance characteristics. The results of variance analysis for the experiment are listed in Table 3. When the *F*-test values of factors and interactions between the factors are smaller than 94% confidence interval, these values are classified as insignificant factors and can be regarded as errors. Therefore, the control factors with the significant effect for acquiring maximal electrical power are A (flow orientation), *B* (temperature of fuel cell), *C* (anode humidification temperature), and *D* (cathode humidification temperature).

4.1.1. Effect of cathode humidification temperature on performance

Fig. 4 shows a trend of better cell performance obtained by a higher cathode humidification temperature. At a fixed anode humidification temperature, a higher water concentration within the membrane can be found in a system with a higher cathode humidification temperature due to strong back-diffusion from the cathode to the anode. However, the cell performance increases for the cathode humidification temperature in the range of 333–353 K. For the cathode humidification temperature at 353 K, the amount of water supplied to the cathode increases more and leads to water flooding. Accordingly, the ANOVA table presents the highest performance at the cathode humidification temperature of 333 K.

4.1.2. Effect of operating temperature on cell performance

The operating temperature is also a significant factor as shown in the ANOVA table. Fig. 5 presents how the cell temperature influences the cell performance. The cell performance increases with increasing the cell temperature in the range of 313–333 K because a higher cell temperature may cause higher electrode reaction and transport rates. Nevertheless, as the cell temperature exceeds 333 K, the cell performance drops with an increase in the cell temperature. This implies that the membrane could be dehydrated as the cell temperature is over 333 K. On the other hand, the cell performance change for low current density is small when increasing cell temperature.

4.1.3. Effect of flow orientation on performance

Fig. 6 compares the polarization curves with different flow orientation from the experiment. Higher electrical powers are obtained in the co-flow case than in the counter-flow case at higher current densities. However, as expected, at lower current densities, in the activation loss region, electrical powers are almost the same for co-flow and counter-flow cases. The flow orientation is also a

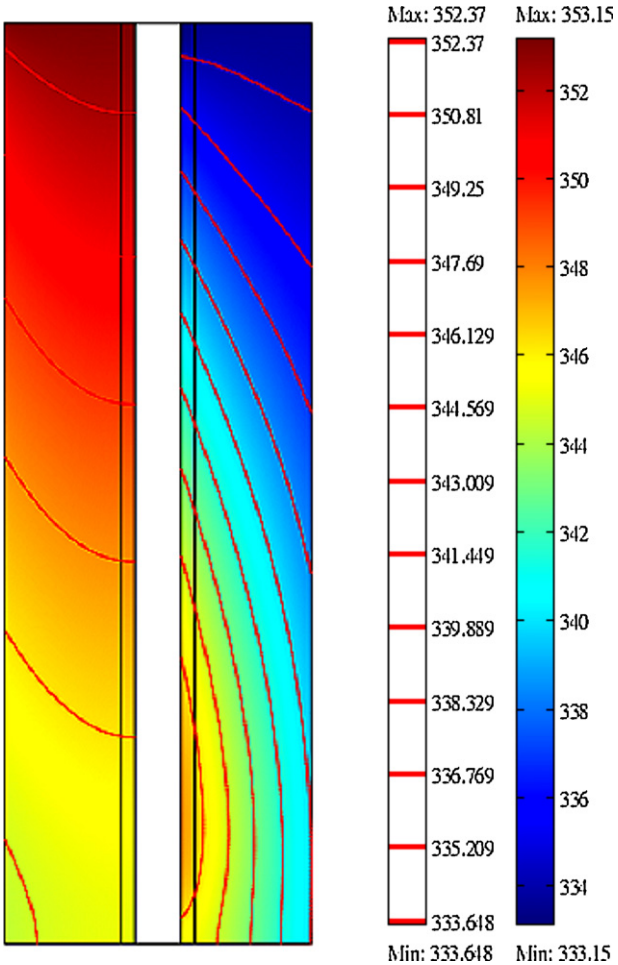

Fig. 11. Temperature distribution for $V_{cell} = 0.5$ V at the optimal condition (*A*1*B*2*C*3*D*2*E*2*F*3).

significant factor as listed in the ANOVA table, but the contribution of the flow orientation (10%) is smaller percentage contribution than that of the cathode humidification temperature and cell temperature.

4.2. Numerical analysis

The governing equations are solved using the general purpose commercial software package COMSOL Multiphysics [19]. COMSOL Multiphysics, a commercial solver by a finite-element technique, is used to solve the governing equations. The UMFPACK direct linear is used in the calculation. All the calculations have been performed by using a PENTIUM 4 4.0G PC. After a series of test runs, a quadrilateral mesh (2835 nodes and 2720 elements) was chosen in all cases. Further refinement changed the current density less than 0.1%. The other two meshes tested were 1952 nodes, 6840 elements and 3807 nodes, 3680 elements as shown in Fig. 7.

The results of simulation on electrochemical behavior of PEM fuel cell are presented by using a single-phase two-dimensional finite-element analysis under the optimal combination factors. The model takes into account the conservation of momentum, current, mass, and thermal energy on the anode and cathode side, as well as conservation of charge throughout the whole cell. In addition to the polarization curve, the model also allows for the assessment of important information about the detail of transport phenomena inside the fuel cell. These transport phenomena are investigated by the velocity vector field, variation of local concentration of gas reactants, and temperature field.

4.2.1. Comparison between numerical and experimental data

The polarization curves obtained from the model for the geometric configuration (Fig. 2) are depicted in Fig. 8, together with the measured polarization curves. The 2D model simulated polarization curves has the same trend with experimental results at the optimal combinations of the control factor levels (*A*1*B*2*C*3*D*2*E*2*F*3). Some difference between experimental and simulation results may be caused using by two-dimensional model approximating the real model of three dimensions with flow channels. Furthermore, the result of the present prediction of the polarization curve has similar trend with that of Shi, Wang, and Zhang's prediction [20], in which their model has channels, as shown in Fig. 9. These results give one confidence in the use of the present program.

4.2.2. Hydrogen and oxygen concentration distribution

Fig. 10 shows the concentration profile of oxygen in the cathode side and hydrogen in the anode side with velocity vectors at the optimal operating conditions. A clear decrease in the concentration of the reactant gas appears along the flow direction and toward the membrane direction due to consumption of the oxygen and hydrogen in the electrochemical reaction at the catalyst layers on both sides. The velocity vectors represent the direction of gas reactants flow, and the length of vector represents the magnitude. At inlets, the magnitudes of velocity for hydrogen in the anode side are larger than those of velocity for oxygen in the cathode side owing to a larger stoichiometric flow ratio of hydrogen from Eq. (23). The contour lines of the reactant concentration show different inclinations: they are sharper in the cathode electrode.

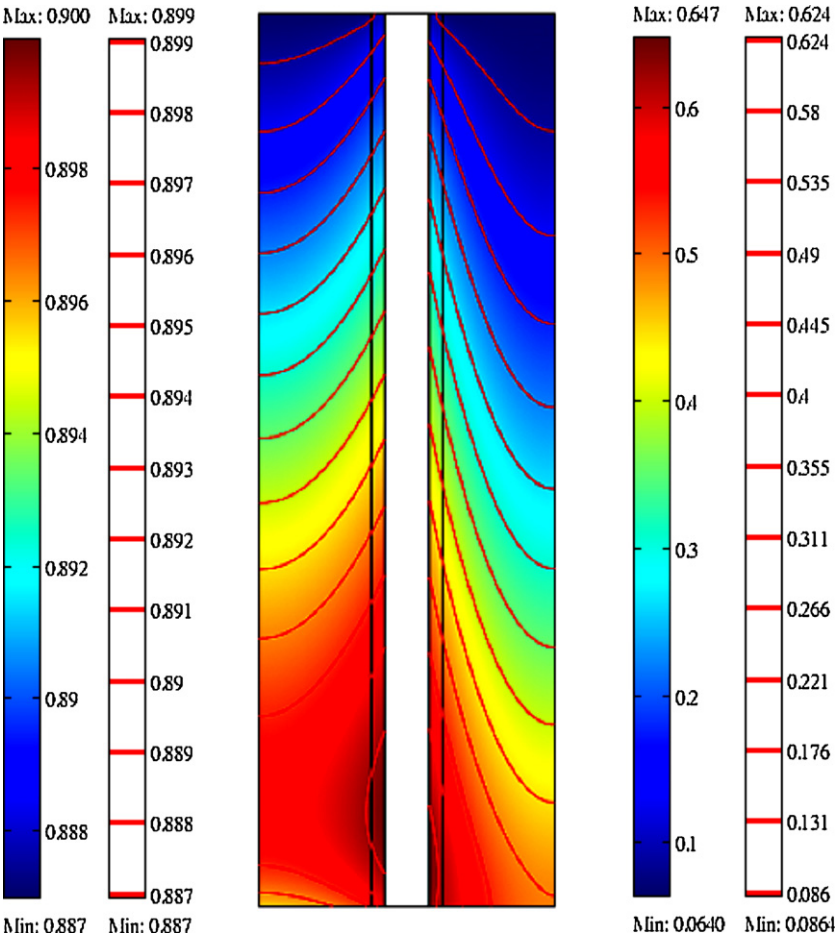

Fig. 12. Water concentration profiles for V_{cell} = 0.5 V at the optimal condition (*A*1*B*2*C*3*D*2*E*2*F*3).

The hydrogen is consumed faster than oxygen due to faster anode electrochemical half reaction than that of cathode side.

4.2.3. Temperature distribution

Temperature distribution for the optimal combinations (*A*1*B*2*C*3*D*2*E*2*F*3) of the control factor levels is demonstrated in Fig. 11. The highest temperature occurs in the cathode catalyst layer where the heat from electrochemical reaction is generated and then the highest water vapor concentration obtained as shown in Fig. 12. The temperatures decrease along the flow direction because of the decreased reactant concentration and the increased water vapor production.

5. Conclusion

The optimization of the operating parameters affecting the performance of PEM fuel cell and obtaining related data is very important in various applications, and in particular for fuel cell producers to validate and improve their models. In the present study, Taguchi method has been used to determine the optimum working conditions for maximum power of a PEM fuel cell. The L_{18} (2×3^7) technique is used for experimental design to reduce the number of experiments required to investigate a set of parameters and to minimize time and cost while performing experiments. Experimental investigations into the parameter effects have allowed determining the optimum configuration of design parameters for maximum power by 17.61 W. Moreover, the ANOVA result indicates that the anode and cathode humidification temperatures, cell temperature, and flow orientation are the significant factors in affecting the PEM fuel cell performance. Higher electrical powers are obtained in the co-flow case rather than in the counter-flow case at higher current densities. The flow orientation is also a significant factor but the contribution of flow orientation (10%) is smaller than that of the cathode humidification temperature and cell temperature. The polarization curve obtained in the simulation is in suitable agreement with that of the experiment and other's prediction. The transport phenomenon by a two-dimensional simulation model is also realized for the fuel cell at the optimal operating condition.

Acknowledgement

The authors would like to acknowledge the financial support of this work by the National Science Council, ROC through the Contract 97-2221-E-006-270-MY3.

References

[1] S. Basu, Recent Trends Fuel Cell Sci. Technol. (2007) P77.
[2] T. Nguyen, R. White, J. Electrochem. Soc. 140 (1993) 2178–2186.
[3] D. Singh, D.M. Lu, N. Djilali, Int. J. Eng. Sci. 37 (1998) 431–452.
[4] J.J. Hwang, J. Power Sources 157 (2006) 85–97.
[5] J.-H. Jang, W.-M. Yan, C.-C. Shih, J. Power Sources 156 (2006) 244–252.
[6] G.H. Guvelioglu, H.G. Stenger, J. Power Sources 163 (2007) 882–891.
[7] S.-W. Perng, H.-W. Wu, J. Power Sources 175 (2008) 806–816.
[8] S. Um, C.-Y. Wang, J. Power Sources 156 (2006) 211–223.
[9] M. Grujicic, K.M. Chittajallu, Appl. Surf. Sci. 227 (2004) 56–72.
[10] M. Grujicic, K.M. Chittajallu, Chem. Eng. Sci. 59 (2004) 5883–5895.
[11] W.-L. Yu, S.-J. Wu, S.-W. Shiah, Int. J. Hydrogen Energy 33 (2008) 2311–2322.
[12] S.-J. Wu, S.-W. Shiah, W.-L. Yu, Renew. Energy 34 (2009) 135–144.
[13] S. Kaytakoğglu, L. Akyalın, Int. J. Hydrogen Energy 32 (2007) 4418–4423.
[14] M.F. Torchio, M.G. Santarelli, A. Nicali, J. Power Sources 149 (2005) 33–43.
[15] R.C. Dante, J.-e.L. Escamilla, V. Madrigal, T. Theuss, J. de Dios Calder'ron, O. Solorza, et al., Int. J. Hydrogen Energy 28 (2003) 343–348.
[16] S. Ghosh, W.R. Schucany, D.B. Owen, W.B. Smith, Stat. Quality (1997).
[17] R.K. Roy, A primer on the Taguchi method, 1990.
[18] J. Bear, J.M. Buchlin, Modeling and Application of Transport Phenomena in Porous Media, Kluwer Academic Publishers, Boston, MA, 1991.
[19] COMSOL Multiphysics Software 3.3, http://www.comsol.com, 2006.
[20] Z. Shi, X. Wang, Z. Zhang, The Proceedings of the COMSOL Users Conference, Boston, 2006.